Available online at www.sciencedirect.com

ScienceDirect

Geochimica et Cosmochimica Acta 214 (2017) 1–13

Geochimica et Cosmochimica Acta

www.elsevier.com/locate/gca

Potassium isotope fractionation between K-salts and saturated aqueous solutions at room temperature: Laboratory experiments and theoretical calculations

Weiqiang Li [a,*], Kideok D. Kwon [b], Shilei Li [a,c], Brian L. Beard [d,e]

[a] State Key Laboratory for Mineral Deposits Research, School of Earth Sciences and Engineering, Nanjing University, Nanjing 210046, People's Republic of China

[b] Department of Geology, Kangwon National University, Chuncheon 24341, Republic of Korea

[c] MOE Key Laboratory of Surficial Geochemistry, School of Earth Sciences and Engineering, Nanjing University, Nanjing 210046, People's Republic of China

[d] Department of Geoscience, University of Wisconsin-Madison, 1215W Dayton Street, Madison, WI 53706, United States

[e] NASA Astrobiology Institute, University of Wisconsin-Madison, Madison, WI, United States

Received 24 February 2017; accepted in revised form 20 July 2017; Available online 28 July 2017

Abstract

Improvements in mass spectrometry have made it possible to identify naturally occurring K isotope ($^{39}K/^{41}K$) variability in terrestrial samples that can be used in a variety of geological and biological applications that involve cycling of K such as clay or evaporite formation. However, our ability to interpret K isotope variability is limited by a poor understanding of how K isotopes are fractionated at low temperatures. In this study, we conducted recrystallization experiments of eight K-salts in order to measure the K isotope fractionation factor between the salt and the saturated K solution ($\Delta^{41}K_{min\text{-}sol}$). Measured $\Delta^{41}K_{min\text{-}sol}$ are +0.50‰ for $K_2CO_3{\cdot}1.5H_2O$, +0.32‰ for K_2SO_4, +0.23‰ for $KHCO_3$, +0.06‰ for $K_2C_2O_4{\cdot}H_2O$, +0.02‰ for KCl, −0.03‰ for K_2CrO_4, −0.15‰ for KBr, and −0.52‰ for KI. Overall the $\Delta^{41}K_{min\text{-}sol}$ decreases with increasing r for K in crystals, where r is the average distance between a K atom and its neighboring atoms of negative charge. Salts with monovalent anions and salts with divalent anion complexes define different linear trends with distinct slopes on a plot of $\Delta^{41}K_{min\text{-}sol}$ - r. We applied *ab initio* lattice dynamics and empirical crystal-chemistry models to calculation of K isotope fractionation factors between K salts; both methods showed that the calculated inter-mineral K isotope fractionation factors ($\Delta^{41}K_{min\text{-}KCl}$) are highly consistent with experimentally derived $\Delta^{41}K_{min\text{-}KCl}$ under the assumption of consistent β factors for different saturated K solutions. Formulations for the crystal-chemistry model further indicate that both anion charge and bond length r are the principle controlling factors for K isotope fractionation, and the K isotope fractionation factors correlate with r following a $1/r^3$ relationship. Our experiment and theoretical study confirms the existence of significant equilibrium K isotope fractionation at ambient conditions, and the K isotope fractionation factors for halides and sulfate obtained in this study provide a basis for future K isotope studies on evaporites.

Keywords: K isotopes; Isotope fractionation; Recrystallization; Evaporites; Ab initio calculation

1. INTRODUCTION

Potassium (K) is an incompatible lithophile element that is progressively concentrated into the crust during planetary

* Corresponding author.
E-mail address: liweiqiang@nju.edu.cn (W. Li).

http://dx.doi.org/10.1016/j.gca.2017.07.037
0016-7037/

differentiation. The K concentrations of the Earth's mantle and crust are estimated at 190–260 ppm and 2.3 wt.%, respectively, making K the fifteenth most abundant element in Earth's mantle and the eighth in the crust (Rudnick and Gao, 2003; Lyubetskaya and Korenaga, 2007; Palme and O'Neill, 2014). As a highly soluble alkaline element, potassium is dissolved into aqueous solutions during silicate weathering, forming a major constituent in river waters (0.2–20 ppm; Meybeck, 2003) and seawater (ca. 400 ppm; Broecker and Peng, 1982). The continental input of K into seawater is balanced by uptake into clay minerals in marine sediments (Michalopoulos and Aller, 1995) and by hydrothermal alteration in mid ocean ridges (Spivack and Staudigel, 1994). The inputs and outputs into seawater result in a mean K residence time of 12 million years in oceans (Broecker and Peng, 1982). In short, partitioning of K between different phases occurs in a variety of processes including hydrothermal alteration, igneous differentiation, and chemical weathering.

Potassium has three naturally occurring isotopes: ^{39}K (93.258%), ^{40}K (0.012%, radioactive, half-life 1.248 billion years), and ^{41}K (6.730%). Variations in $^{41}K/^{39}K$ may be used to track how K is partitioned into different reservoirs in a variety of processes (Teng et al., 2017). The precision of $^{41}K/^{39}K$ ratio measurements in early studies using thermal ionization mass spectrometry (TIMS) and secondary ionization mass spectrometry (SIMS) was at a level of ±1‰ (Barnes et al., 1973; Garner et al., 1975) and ±0.5 ‰ (Humayun and Clayton, 1995a, 1995b; Humayun and Koeberl, 2004), respectively, and was not sufficient to resolve the K isotope variability in terrestrial rocks, which was estimated to be at the sub per mil level (Humayun and Clayton, 1995b). Recent studies, however, have used multi-collector inductively coupled plasma mass spectrometry (MC-ICP-MS) to improve the precision of K isotope measurements to a level of <0.1 ‰ for $^{41}K/^{39}K$ ratios (Li et al., 2016; Wang and Jacobsen, 2016a). With this improved precision, it has been possible to identify that seawater is isotopically heavier than igneous rocks by 0.6 ‰ in $^{41}K/^{39}K$ (Li et al., 2016; Wang and Jacobsen, 2016a), and altered basalts at mid-ocean ridge were found to have higher $^{41}K/^{39}K$ ratios that are more similar to seawater (Parendo et al., 2017). Lunar rocks are also isotopically heavier than the bulk silicate earth by 0.4–0.6 ‰ in $^{41}K/^{39}K$ (Wang and Jacobsen, 2016b). In addition, analyses of biological samples have revealed a > 2.4‰ variation in $^{41}K/^{39}K$ in organisms. For example, terrestrial higher plants tend to enrich light K isotopes whereas sea algaes tend to enrich heavy K isotopes (Li et al., 2016; Li, 2017). Despite the relatively limited number of K isotope studies, K isotopes have demonstrated great potential as a novel geochemical tool for a wide range of research topics.

Interpretation of the natural variations of K isotope compositions requires an understanding of the controlling factors of K isotope fractionation between different K phases (i.e., minerals, aqueous solutions, and vapor). For example, the recent discovery of heavier K isotope compositions of lunar rocks places important constraints on the giant-impact origin for the Moon (Wang and Jacobsen, 2016b), and much of the interpretation of heavy K isotope signature in lunar rocks was based on existing experimental results of vaporization of K at different vapor pressures (Richter et al., 2011). On the other hand, the 0.6‰ difference in $^{41}K/^{39}K$ between seawater and igneous rocks implies that global cycling of K is associated with K isotope fractionation. However, the cause of enrichment of heavy K isotopes in seawater is poorly understood, and currently the interpretation of K isotope variability in terrestrial samples is challenging because there is limited information regarding the partitioning behavior of K isotopes between minerals and aqueous solutions.

In this study, we aimed to understand the controlling factors of K isotope fractionation between aqueous solutions and minerals at ambient conditions, and measured K isotope fractionation factors between eight K-bearing salts and the respective salt-saturated aqueous solutions at room temperature. Three of the studied salts are K halides (KCl, KBr, and KI), which are isostructural in crystal lattice, but have progressively longer K-halogen bonds. Other salts include dipotassium carbonate sesquihydrate ($K_2CO_3 \cdot 1.5H_2O$) and potassium bicarbonate ($KHCO_3$), K sulfate (K_2SO_4), K chromate (K_2CrO_4), and a K salt of organic acid ($K_2C_2O_4 \cdot H_2O$). These minerals have a variety of lattice structures, K bonds, and include both divalent and monovalent anion complexes and therefore provide a test of the effects of ion bonding on isotopic fractionation in ionic crystals. The inter-mineral K isotope fractionation factors were further investigated by theoretical calculations using two different methods to compare with the experimental results. Notably, because KCl and K_2SO_4 are important constituents in evaporites, the K isotope fractionation factors for the two minerals provide important constraints for interpretation of K isotope data from natural evaporites.

2. METHODS

2.1. Recrystallization experiments

Fine crystals of reagent grade KCl, KBr, KI, K_2CrO_4, $K_2C_2O_4 \cdot H_2O$, K_2CO_3, $KHCO_3$, and K_2SO_4 (purchased from Shanghai Lingfeng Chemical Reagent Co. Ltd.) were used for recrystallization experiments. For each experiment, a saturated salt solution was firstly prepared by dissolving 5–10 g of the salt in approximately 7 mL deionized water (>18.2 Ω) in a 15 mL plastic centrifuge tube, when saturation was reached, additional 1–2 g of salt was added into the centrifuge tube to produce an apparent volume ratio of 4:1 to 5:1 (estimated based on the gradations on the centrifuge tube) between the saturated fluid and crystals. Centrifuge tubes were tightly capped and the contents were well mixed using a roller to rotate the tube at 10 rotations per minute. To prevent decomposition of KI by light, the centrifuge tube containing KI was thoroughly wrapped with two layers of Aluminum foil. The experiments were done at room temperature (air-conditioned to 25 ± 2 °C) and after aging for 3 months at State Key Laboratory for Mineral Deposit Research, Nanjing University, the tubes were harvested for an aliquot of the saturated K solution and recrystallized salt. These samples were collected by allowing

the contents of the tube to settle for over 5 min and an aliquot of clear aqueous solution was collected using a pipettor for K isotope analysis. The remaining solution was removed using a pipettor, leaving crystals and interstitial fluid in the centrifuge tube. The crystals with interstitial fluid were quickly dumped onto a thick pile (>10 layers) of Kimwipes® paper wipers and the pile was gently pressed with the wipers so that the interstitial fluid was absorbed by the wipers, leaving dry clean crystals. Crystals were then handpicked for XRD analysis and K isotope analysis.

2.2. XRD analysis

Powder X-ray diffraction analysis of recrystallized minerals was performed on a Rigaku Rapid II dual-source X-ray Diffractometer at State Key Laboratory for Mineral Deposit Research, Nanjing University. The instrument was operating with a rotating anode Mo target X-ray source (Mo $K_\alpha = 0.71073$ Å) running at 40 kV and 90mA, and 5 min exposure was used for each sample. Diffraction data were collected on a 2-D image plate detector, and were converted to produce conventional 2θ vs. intensity patterns using Rigaku 2DP software. Data processing and mineral identification were made using Jade 6.5 and a PDXL software.

2.3. K isotope analysis

2.3.1. Sample preparation and purification

Sample preparation was undertaken at Nanjing University, where all chemical procedures were performed in a clean room with laminar flow hoods and HEPA filtered air. Deionized (18.2 MΩ) water, Teflon-coated hot plates, Teflon beakers, double distilled reagents were used throughout the experiments; other labware, such as centrifuge tubes and pipette tips, were soaked in 6 M HCl overnight and rinsed using deionized water before usage. An aliquot of the dissolved sample that typically contained 50–200 μg of K was treated by repeatedly drying and redissolution in 50–100 μL concentrated HNO_3. The sample was subsequently dried and dissolved in 0.5 mL 1.5 M HNO_3, and ready for chemical purification using ion exchange chromatography.

Separation of K from matrix elements followed a two-stage ion exchange protocol that has been described in Li et al. (2016). A dissolved sample was loaded on to a first-stage column that contained 1 mL wet volume (in deionized water, gravity packing) of 100–200 mesh BioRad® AG50 W-X12 resin and eluted using 1.5 M HNO_3. Unwanted anions such as SO_4^{2-} and CrO_4^{2-} were eluted off the column in the first 1–2 mL of 1.5 M HNO_3. Effective separation of K from other trace matrix elements was achieved using the first stage column. The K-bearing solution collected from first stage column was further purified through a second stage column that contained 0.4 mL wet volume of 100–200 mesh BioRad® AG50W-X8 resin, using a series of weak acids (Li et al., 2016). This two-stage column results in K recovery of 99.4 ± 2.1% (2SD, n = 54), and a total procedural K blank of 3–8 ng (n = 5), which is negligible compared with the >50 μg of K in each sample.

2.3.2. Mass spectrometry

$^{41}K/^{39}K$ isotope ratio measurements were performed on a Micromass IsoProbe MC-ICP-MS at the University of Wisconsin – Madison, using instrument settings that have been detailed in Li et al. (2016). The IsoProbe MC-ICP-MS was run with a standard 1350 W forward RF power, using high purity He (flow rate: 10 mL/min) as the collision gas and high purity D_2 (flow rate: 6 mL/min) as the reaction gas. Argon hydride ($^{40}ArH^+$), which is the most difficult isobar to remove from the K mass spectrum is nearly quantitatively suppressed via proton transfer and atom transfer reactions with D_2 in the collision cell (Li et al., 2016). Potassium solutions were introduced into the plasma using a self-aspirating Glass Expansion Micromist nebulizer with an uptake rate of ~0.1 mL/min and a Glass Expansion Cyclonic spray chamber cooled to 5 °C using a water jacket. Typical sensitivity for 1 ppm K solution under standard mass resolution (~400 resolving power) was 7–11 V on ^{39}K and 0.6–1 V on ^{41}K.

A standard-sample-standard bracketing routine was applied for K isotope ratio measurement, against a 1 ppm in-house K stock solution (UW-K). Sample solutions were diluted to match the concentration of standard solution to better than ±10%. A 60 s on-peak acid blank was measured prior to each isotopic analysis of K solution, and was subtracted from the analyte signal. Each K isotopic analysis consisted of forty 5 s integrations.

2.3.3. Data reporting, precision, and accuracy

Potassium isotope compositions are reported using the standard per mil (‰) notation of $\delta^{41}K$ for a $^{41}K/^{39}K$ ratio, where

$$\delta^{41}K = [(^{41}K/^{39}K)_{sample}/(^{41}K/^{39}K)_{standard} - 1] \times 1000 \quad (1)$$

Fractionation in K isotopes between two phases A and B is expressed as:

$$\Delta^{41}K_{A-B} = \delta^{41}K_A - \delta^{41}K_B \approx 10^3 \ln \alpha_{A-B}^{41/39} \quad (2)$$

The error in K isotope fractionation factors is calculated by the error propagation function:

$$Err\Delta K_{A-B} = [(Err\delta K_A)^2 + (Err\delta K_B)^2]^{1/2} \quad (3)$$

where $Err\Delta K_{A\text{-}B}$ is the error of K isotope fractionation factor, and $Err\delta K_A$ and $Err\delta K_B$ are the analytical errors for phase A and B, respectively.All K isotope data are reported relative to NIST SRM 3141a which is a K solution with a certified 10,000 ppm K concentration. The in-house K stock solution (UW-K) has a $\delta^{41}K$ value of −0.11 ± 0.02‰ (2 standard error, or 2SE, $n = 100$) relative to NIST SRM 3141a; seawater has a $\delta^{41}K$ value of 0.06 ± 0.10‰ (2 standard deviation, or 2SD, $n = 3$) (Li et al., 2016). In a recent study by Wang and Jacobsen (2016a), K isotopic data were reported against a Bulk Silicate Earth (BSE) value that was defined by the average K isotopic composition of three basalt samples. On the Bulk Silicate Earth scale, seawater has $\delta^{41}K$ value of 0.58 ± 0.07‰

(Wang and Jacobsen, 2016a), therefore there is a 0.52‰ offset in $\delta^{41}K$ between the proposed BSE value and NIST SRM3141a. Correction of such offset is applied in subsequent discussions where K isotopic data reported by Wang and Jacobsen (2016a) is included.

Internal precision for $^{41}K/^{39}K$ ratio measurement of the method was better than ±0.07‰ (2SE), mostly better than ±0.04‰ (2SE). Long-term external reproducibility of $^{41}K/^{39}K$ ratio measurement was monitored by repeat analysis of NIST SRM 3141a against in-house K stock solution (UW-K), and was ±0.19‰ (2SD, $n = 100$) over two years. Accuracy of the method was checked by analyzing pure NIST 3141a K and synthetic samples that were treated as samples using the two-stage ion exchange columns. The synthetic samples were made by mixing UW-K solution with matrix elements separated from different natural samples during ion exchange column chemistry. The measured $\delta^{41}K$ values for five processed NIST 3141a K cluster around 0‰ (-0.03 ± 0.13‰, 2SD, $n = 5$), and the measured $\delta^{41}K$ values for seven synthetic samples that were doped with UW-K cluster around −0.12‰ (−0.10 ± 0.08‰, 2SD, $n = 7$) (Li et al., 2016). An additional accuracy check is the consistency of $\delta^{41}K$ value difference between seawater and igneous rocks (e.g., BHVO-1 and BHVO-2), which is reported to be 0.58‰ in Wang and Jacobsen (2016a) and 0.56‰ in Li et al. (2016).

2.4. Theoretical calculations

Equilibrium isotope fractionation arises from differences in vibrational frequencies by isotopic substitution (Bigeleisen and Mayer, 1947; Schauble, 2004; Young et al., 2015). Isotopic fractionation factor between phase A and phase B at equilibrium ($\alpha_{A\text{-}B}$) can be defined with the reduced partition function ratios (RPFR or β-factor):

$$\alpha_{A-B} = \beta_A/\beta_B \tag{4}$$

where β_A and β_B are the beta factor of phase A and B, respectively. Under the harmonic approximation with the high-temperature product rule (Bigeleisen and Mayer, 1947; Kieffer and Werner, 1982; Dove, 1993; Schauble, 2004; Young et al., 2015), the β-factor of a periodic phase like a mineral can be calculated by a following equation,

$$\beta = \left[\prod_{i=1}^{3N_{at}}\prod_{q}\frac{v^*_{q,i}}{v_{q,i}}\frac{e^{-hv^*_{q,i}/(2kT)}}{1-e^{-hv^*_{q,i}/(kT)}}\frac{1-e^{-hv_{q,i}/(kT)}}{e^{-hv_{q,i}/(2kT)}}\right]^{1/(N_qN)} \tag{5}$$

where v is a harmonic vibrational frequency of the i^{th} vibrational mode at a phonon wave vector q; h, k_B, and T are Planck constant, Boltzmann constant, and the absolute temperature in Kelvin, respectively; N_{at}, N_q, and N represent the number of atoms in a unit cell, phonon wave vectors, and sites of isotopes, respectively (Schauble et al., 2006; Blanchard et al., 2009). The * represents a frequency for a heavier isotope, and three acoustic vibrational modes at the gamma point with a frequency of zero are not considered in the β-factor calculations.

Approaches to derive β factors include acquisition of the complete spectrum of vibrational motions by *ab initio* lattice dynamics calculations or by spectroscopic measurements such as nuclear resonance inelastic X-ray scattering (NRIXS). Additionally, empirical methods based on crystal-chemistry models can also be used to calculate inter-mineral isotope fractionation factors (Young et al., 2002, 2009, 2015). In this study, we applied the *ab initio* method to calculate the K isotope fractionation factors of K salts, and we also utilized the empirical method for KCl, KBr, and KI. These two different methods are complimentary and provide different perspectives for understanding the K isotope fractionations.

2.4.1. *ab initio* calculations

The *ab initio* lattice dynamics with the harmonic approximation was performed based on density functional theory (DFT), using CASTEP, a plane-wave pseudopotential DFT code (Clark et al., 2005), within the general gradient approximation for electron correlation using the Perdew, Burke and Ernzerhof functional (Perdew et al., 1997). Norm conserving pseudopotentials (Kleinman and Bylander, 1982) were used to describe the strong Coulomb potentials between atomic nuclei and core electrons. The valence electron configurations for the C, O, S, K, Cl, Br, and I pseudopotentials were $2s^22p^2$, $2s^22p^4$, $3s^23p^4$, $3s^23p^64s^1$, $3s^23p^5$, $3d^{10}4s^24p^5$ and $5s^25p^5$, respectively. The plane-wave basis sets were expanded until the kinetic energy was lower than 1,400 eV. The first Brillouin zone was sampled with a 7 × 7 × 7 grid in k space (Monkhorst and Pack, 1976) for the primitive halide cells, a 5 × 3 × 4 k-point grid for $K_2CO_3{\cdot}1.5H_2O$, and a 4 × 3 × 5 k-point grid for K_2SO_4 unit cell. These cutoff energy and k-point grid were chosen such that the atomic force converged to much less than 0.001 eV/Å; tests for KCl showed that the vibrational frequencies converged to less than 0.5 cm^{-1}. The geometry optimizations followed the BFGS procedure (Pfrommer et al., 1997) with correction for finite basis set error (Francis and Payne, 1990).

We used density functional perturbation theory (DFPT) (Baroni et al., 2001; Refson et al., 2006) to calculate the harmonic vibrational frequencies, which are the eigenvalues of dynamical matrices. A dynamical matrix is the mass-reduced Fourier transform of an interatomic force constant matrix. In *ab initio* lattice dynamics, the force constants are in the form of the second derivatives of the total energies with respect to atom displacements. The Hellmann-Feynmann Theorem ensures that the force constant solution needs only first-order derivatives of wave functions (i.e., linear electronic response of a system). In DFPT, the derivatives are evaluated using standard perturbation theory and ground-state Khon-Sham orbitals (Baroni et al., 2001; Refson et al., 2006). This approach, also called a linear response method, enables one to calculate phonons at any wave vector using a primitive-cell, differently from the finite displacement method using numerical derivatives with supercells (Ackland et al., 1997). In DFPT, the dynamical matrix is computed calculating the linear response orbitals based on a relatively coarse grid of phonon wave vectors (q), and then Fourier interpolation is used to obtain dynamical matrices at a finer gird of q points; diagonalization of the dynamical matrices gives frequencies at the finer grid.

A sufficiently large number of phonon wave vectors (N_q) should be used in the beta-factor calculations (Eq. (5)). In the K halide calculations, we used harmonic frequencies obtained by Fourier interpolation at a $7 \times 7 \times 7$ q-point grid ($N_q = 25$) of the dynamical matrices which were directly calculated at a $5 \times 5 \times 5$ q-point grid. In $K_2CO_3 \cdot 1.5H_2O$ calculation, four irreducible q points were used without interpolation at a fine grid. For K_2SO_4, $3 \times 3 \times 2$ and $5 \times 7 \times 3$ grids were used for the coarse and fine q-point grids, respectively, including the gamma point. In order to evaluate whether the current use of N_q is sufficient, or the calculated beta-factor is well converged with respect to N_q, we calculated the beta-factor of KCl by using a very large q-point grid: a $13 \times 13 \times 13$ grid for the direct dynamical matrix calculation and a $25 \times 25 \times 25$ grid ($N_q = 455$) for the Fourier interpolation. Convergence testing of the carbonate hydrate mineral is prohibitively expensive. The 1000lnβ of KCl calculated with the large grid differed by +0.036‰ at 300 K from the current value (Appendix 1; Fig. S1), which can be used as the precision of our current DFT method for beta-factors.

2.4.2. Empirical calculations

Previous researchers have applied a number of different mathematical treatments to calculate β values (Bigeleisen and Mayer, 1947; Urey, 1947; Young et al., 2015), but all concluded that the β factor in Eq. (5) can be approximated by:

$$\beta = 1 + \frac{1}{24}\sum_i (u_i^2 - u_i'^2) \tag{6}$$

by treating the vibrations (u_i) as harmonic and introducing the average force constant $\hat{K}$ for the site in question, Young et al. (2002, 2009, 2015) further derived:

$$\ln \alpha_{A-B} = \frac{1}{24}\left(\frac{h}{K_b T}\right)^2 \left(\frac{1}{m} - \frac{1}{m'}\right)\left[\frac{\hat{K}_{f,A}}{4\pi^2} - \frac{\hat{K}_{f,B}}{4\pi^2}\right] \tag{7}$$

$\hat{K}$ is the second order derivative of lattice energy E, which can be described using Born-Mayer equation (Born and Mayer, 1932).

$$\hat{K} = \frac{d^2E}{dr^2} = d^2\left[\frac{MZ^+Z^-}{r}\left(\frac{e^2}{4\pi\varepsilon_0}\right) + \frac{B_c}{r^n}\right] \Big/ dr^2 \tag{8}$$

where M is Madelung constant, Z^+ and Z^- are the cation and anion valences, e is the charge of an electron, ε_0 is vacuum permittivity, B_c is a constant specific to the bond in crystal and n is the exponent constant also to the bond type.

B_c could be reduced because the first order derivative of lattice energy is zero when $r = r_0$, so

$$\left(\frac{dE}{dr}\right)_{r_0} = \frac{-MZ^+Z^-}{r_0^2}\left(\frac{e^2}{4\pi\varepsilon_0}\right) - \frac{nB_c}{r_0^{n+1}} = 0 \tag{9}$$

Combining Eqs. (8) and (9), B_c is canceled and we have

$$\hat{K} = \frac{Z^+Z^-Me^2}{4\pi\varepsilon_0}\frac{(1-n)}{r_0^3} \tag{10}$$

K isotope fractionation factors between K halides can be calculated by combining Eqs. (7) and (10). The input data include r_0, n, and M. r_0 is the inter-atomic distance between K and neighboring halide anion, which is available from X-ray diffraction studies (Ahtee, 1969; Walker et al., 2004). The exponents constant n in the Born-Mayer equation for different minerals are tabulated in Ruffa (1980). M, the Madelung constant, is dependent on crystal structure, and is 1.748 for NaCl-type structure including KCl, KBr, and KI (Sakamoto, 1958).

3. RESULTS

3.1. Experimental results

XRD analyses confirmed that the mineralogy of the salts remained unchanged after the recrystallization experiments (Appendix 1), with an exception of K_2CO_3, which incorporated H_2O molecules into the crystal lattice and transformed to dipotassium carbonate sesquihydrate ($K_2CO_3 \cdot 1.5H_2O$; Appendix 1). The starting K_2CO_3 crystals were very fine and highly hydroscopic, and commonly formed agglomeritic masses (Fig. 1), after the recrystallization experiments, $K_2CO_3 \cdot 1.5H_2O$ crystals with rhomboid crystal behaviors were formed. The other K-salts before exposure to the saturated K solutions typically had crystal habits that were similar to the recrystallized salts. The halide salts had cubic habits with the KCl having the most euhedral crystals and the KBr and KI having subhedral crystals. The recrystallized halide salts displayed rounding and were more subhedral and anhedral than the starting salt crystals (Fig. 1). The rest of K bearing salts (K_2CrO_4, $K_2C_2O_4 \cdot H_2O$, $KHCO_3$, and K_2SO_4) were mixtures of prismatic and subhedral to anhderal rhomboids whereas the recrystallized salts tended to be rhombohedral shaped with significant rounding (Fig. 1). Starting salt crystals were typically less than 1000 μm and were smaller than the recrystallized salts (Table 1). For example, the typical size of $K_2C_2O_4 \cdot H_2O$ crystals increased from 500 μm to 5000 μm, whereas the typical size of KCl crystals increased from 200 μm to 1500 μm. We note that the rounding in the recrystallized salt crystals may reflect both recrystallization processes as well as physical abrasion in the rolling tubes that was done to keep the solutions well mixed.

Based on K isotope compositions of solid and liquid phases, the apparent K isotope fractionation factors ($\delta^{41}K_{solid}$-$\delta^{41}K_{aquous}$) between solid and aqueous phases were obtained (Table 1; Fig. 2). Potassium in recrystallized $K_2CO_3 \cdot 1.5H_2O$, K_2SO_4, and $KHCO_3$ were isotopically heavier than their respective saturated aqueous solutions by 0.50‰, 0.32‰, and 0.23‰, respectively. The $\delta^{41}K$ values of recrystallized KCl, $K_2C_2O_4 \cdot H_2O$, and K_2CrO_4 crystals were analytically indistinguishable from their respective aqueous solutions with in ±0.10‰. By contrast, recrystallized KBr and KI crystals were isotopically lighter than their respective saturated solutions by 0.15‰ and 0.52‰, respectively.

3.2. Results of theoretical calculations

3.2.1. ab initio calculations

The harmonic phonon frequencies were calculated based on geometry-optimized crystal structures of potassium salts. The calculated structure parameters matched well

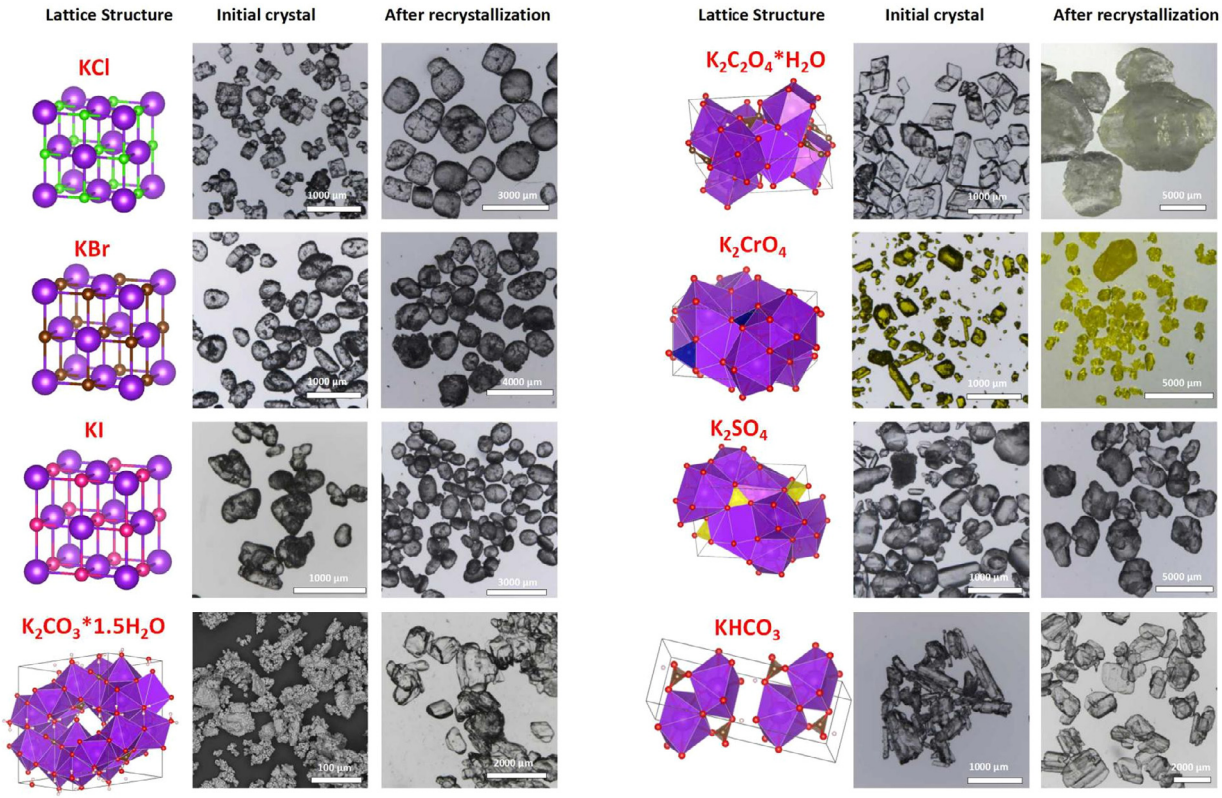

Fig. 1. Photomicrographs of representative crystals before and after recrystallization experiments. All photos were taken under an optical microscope except for initial crystals of K_2CO_3, which was taken using a SEM because the crystals are very fine and hydroscopic, also note this mineral was transformed to K_2CO_3*1.5H_2O during the recrystallization experiment in aqueous solution, for details see text and appendix. The mineralogy of other K-salts The lattice structures of the minerals are also shown with the salt crystal photos, where K atoms are denoted by purple spheres or polyhedron.

with experimental data (Table 2), except for a very small but systematic overestimating tendency that is typical for DFT/PBE method. Accordingly, the calculated phonons tended to be lower than experiment, but they well reproduced the experimental trends of phonon dispersion relations (Appendix 1; Fig. S2). In the potassium halides, as the mass difference between potassium and halide increases (i.e., KCl < KBr < KI), the overall phonon frequencies become lower and the gap increases between the lower end of optical branches and the upper end of acoustic ones. Table 2 lists the calculated frequencies of longitudinal optical and degenerate transverse optical modes for K halides only at the gamma point. For K_2CO_3·1.5H_2O and K_2SO_4, experimental phonon dispersion data are limited to compare with. When compared to Raman data, the calculated frequencies of the carbonate and sulfate also tended to be lower than the experimental results (Appendix 1; Table S1), as in halides.

The isotopic fractionation factors obtained using calculated harmonic frequencies showed a consistent result with the trend observed in our experiment (Table 3; Fig. 3). We note in passing that in the beta-factor calculation, we did not use any scaling factor to the *ab initio* phonon frequencies. In general, potassium beta-factor for the salts follows the order of KI < KBr < KCl < K_2SO_4<K_2CO_3·1.5H_2O; with reference to KCl, the inter-mineral K isotope fractionation factors ($10^3\ln\alpha$) derived from the calculated β factors were −0.45‰ for $\ln\alpha_{KI\text{-}KCl}$, −0.22‰ for $\ln\alpha_{KBr\text{-}KCl}$, +0.19‰ for $\ln\alpha_{K2SO4\text{-}KCl}$, and +0.67‰ for $\ln\alpha_{K2CO3\cdot1.5H2O\text{-}KCl}$ at 25 °C (Fig. 3B; Table 3).

3.2.2. Empirical calculations

Using Eq. (10) and the input parameters for the empirical method, the force constants on K atom are calculated at 64.68 N/m for KCl, 58.38 N/m for KBr, and 49.89 N/m for KI. Using Eq. (7) and the calculated force constants, β factors are calculated for the three halides (Table 3), which are plotted against temperature in Fig. 3A. Inter-mineral K isotope fractionation $10^3\ln\alpha$ can be derived from the calculated β factors, which are −0.22‰ for $\ln\alpha_{KBr\text{-}KCl}$, −0.52‰ for $\ln\alpha_{KI\text{-}KCl}$, and 0.30‰ for $\ln\alpha_{KBr\text{-}KI}$ at 25 °C (Fig. 3B; Table 3).

4. DISCUSSION

4.1. Attainment of isotopic equilibrium in recrystallization experiments

There was a significant increase in crystal size over the course of the recrystallization experiments, where the typi-

Table 1
Summary of recrystallization experiments.

Mineral	Grain size Before recrystallization (μm)	Grain size after recrystallization (μm)	Average bond length for K in mineral (Å)	δ^{41}K of mineral after recrystallization (‰)			δ^{41}K of aqueous solution after recrystallization (‰)			$\Delta^{41}K_{min\text{-}aq}$ factor (‰)	
				Average	2SD	n	Average	2SD	n	Average	2SD
KCl	200–500	800–2000	3.14	0.13	0.11	6	0.11	0.05	2	0.02	0.12
KBr	300–800	1000–2000	3.29	−0.06	0.15	6	0.09	0.12	7	−0.15	0.20
KI	100–700	800–2000	3.53	−0.49	0.04	2	0.03	0.13	6	−0.52	0.13
$KHCO_3$	200–1000	500–2000	2.84	−0.05	0.10	3	−0.28	0.05	2	0.23	0.12
$K_2C_2O_4*H_2O$	200–1000	3000–10000	2.93	0.27	0.21	7	0.21	0.19	2	0.06	0.28
K_2CrO_4	80–1000	300–3000	2.97	0.20	0.08	5	0.23	0.09	6	−0.03	0.12
K_2SO_4	100–1000	1000–4000	2.87	0.50	0.19	6	0.18	0.09	4	0.32	0.21
$K_2CO_3{\cdot}1.5H_2O$	Not available	400–1500	2.84	0.59	0.17	4	0.09	0.02	2	0.50	0.17

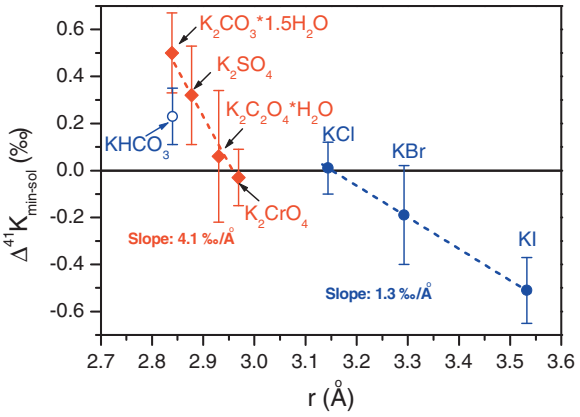

Fig. 2. Plot of Δ^{41}K fractionation factors versus the average distance (r) between K atoms and the nearest atoms of negative charge such as halogen and oxygen in lattice of the minerals.

cal size of crystal salts increased by roughly 4–10 times after three months (Table 1; Fig. 1). The growth of larger crystals was at the expense of dissolution of smaller crystals that tend to have higher surface energy, and this process is termed Ostwald ripening (e.g., Stoffregen et al., 1994; Li et al., 2011). Total volume of crystals before and after each experiment did not change because they equilibrated with the saturated aqueous solution at a constant temperature, and the K concentrations in saturated K-salt solutions remained constant during the recrystallization experiments (Appendix 1; Fig. S3). There was a 4–10-fold increase in crystal size, which can only be accomplished by a decrease in number of total salt crystals by a factor of 64–1000 times, assuming a cubic crystal morphology. In other words, 63/64 to 999/1000 of the initial crystals in the recrystallization experiments had exchanged with the aqueous solution through a dissolution-reprecipitation process. Therefore, it is estimated that near complete (>98%) isotope exchange was achieved in the experiments presented in this study.

Because there was near-complete isotope exchange between the salt crystals and aqueous solutions during recrystallization, it is likely that these experiments represent equilibrium isotopic fractionation between the K salt and aqueous K. Chemical reactions, including isotope exchange, are controlled by the slowest rate among the basic processes (Lasaga, 1981). Mineral-water surface reactions are dynamic and consist of a series of basic processes at the atomic scale, including (1) transport of ions through solution, and (2) adsorption/desorption, dehydration/hydration, and attachment/detachment ions to mineral lattice (Lemarchand et al., 2004; DePaolo, 2011). These processes are termed a "transport process" and "surface processes" (Lasaga, 1990), respectively. It has been well-documented that dissolution reactions of minerals with low solubility are limited by surface processes whereas dissolution reactions of minerals with high solubility are limited by transport process (Berner, 1978; Lasaga, 1990). The eight K salts investigated in this study are all highly soluble (solubility > 1 mol/Liter), and thus recrystallization is controlled by transport processes (Berner, 1978; Lasaga, 1990). Because the recrystallization experiments were con-

Table 2
Structure parameters of potassium salts and halide phonons at the gamma point calculated by using density functional theory (DFT).

	Lattice parameter (Å)		Interatomic distance[a] (Å)		Phonons (cm^{-1})	
	DFT	Exp[b]	DFT	Exp[b]	DFT	Exp[b]
KCl	6.372	6.29	3.17	3.15	196 124	213 147
KBr	6.698	6.6	3.35	3.3	151 100	167 120
KI	7.172	7.07	3.59	3.54	127 88	143 107
K_2SO_4	7.598 10.268 5.879 *120.7	7.476 10.071 5.763 *120.8	2.82 3.01	2.77 2.93		
K_2CO_3·1.5H_2O	12.211 13.771 7.263	11.818 13.747 7.109	2.81 2.88 2.89	2.74 2.81 2.84		

See Fig. S2 for phonon relations and Table S1 for Raman frequencies of K_2SO_4. *Beta angle.
[a] Distance between K and halogen in halides or average distance between K and O in K_2CO_3·1.5H_2O or K_2SO_4.
[b] Experimental data: Mei et al. (2000) and referenced therein for halides; Skakle et al. (2001) for *C*2/*c* K_2CO_3·1.5H_2O; McGinnety (1972) for *Pnam* K_2SO_4.

Table 3
Comparison of reduced partition function ratios (RPFR or β-factor) and inter-mineral K isotope fractionation factors ($\alpha_{A\text{-}B}$) derived from *ab initio* calculations, empirical crystal chemistry models, and experiments.

	RPFR or β-factor function (‰)		1000lnβ @ 25 °C (‰)		
	Ab initio calculation	Empirical crystal chemistry model	*Ab initio* calculation	Empirical crystal chemistry model	
KCl	$1000\ln\beta = 0.1338 * 10^6/T^2$	$1000\ln\beta = 0.2050 * 10^6/T^2$	1.51	2.31	
KBr	$1000\ln\beta = 0.1145 * 10^6/T^2$	$1000\ln\beta = 0.1850 * 10^6/T^2$	1.29	2.08	
KI	$1000\ln\beta = 0.0940 * 10^6/T^2$	$1000\ln\beta = 0.1581 * 10^6/T^2$	1.06	1.78	
K_2SO_4	$1000\ln\beta = 0.1507 * 10^6/T^2$		1.70		
K_2CO_3·1.5H_2O	$1000\ln\beta = 0.1935 * 10^6/T^2$		2.18		
	Inter-mineral fractionation or α-factor (‰)		1000lnα @ 25 °C (‰)		
	Ab initio calculation	Empirical crystal chemistry model	*Ab initio* calculation	Empirical crystal chemistry model	Experiment
KI-KCl	$1000\ln\alpha = -0.0334 * 10^6/T^2$	$1000\ln\alpha = -0.0469 * 10^6/T^2$	−0.45	−0.53	−0.54 ± 0.18
KBr-KCl	$1000\ln\alpha = -0.0193 * 10^6/T^2$	$1000\ln\alpha = -0.0200 * 10^6/T^2$	−0.22	−0.23	−0.17 ± 0.23
K_2SO_4-KCl	$1000\ln\alpha = +0.0169 * 10^6/T^2$		+0.19		+0.30 ± 0.24
K_2CO_3·1.5H_2O -KCl	$1000\ln\alpha = +0.0603 * 10^6/T^2$		+0.67		+0.48 ± 0.21

ducted with active mechanical mixing of the solution and salt crystals it is likely these experiments represent equilibrium isotope exchange. This is analogous to similar Mg isotope experiments conducted using epsomite ($MgSO_4$·7H_2O). Like K salts, epsomite has a high solubility and is classified to the transport controlled category (Berner, 1978; Lasaga, 1990). Systematic experiments using ^{25}Mg-enriched tracer and multiple-direction, variable rate conditions at different temperatures have rigorously proven that equilibrium Mg isotope fractionation for epsomite was achieved within two weeks of recrystallization (Li et al., 2011). The analogy between epsomite and K-salts in this study support attainment of equilibrium fractionation between K salts and saturated solutions after three months, although we note that attainment of isotopic equilibrium could be further supported by time series K isotope data, which are lacking in this study.

4.2. Crystal-chemistry control of K isotope fractionation in salts

There is an approximately 1‰ range in the K isotope fractionation factors between K-salts and the respective saturated aqueous solutions, where for example the $^{41}\Delta K_{min\text{-}aq}$ varied from −0.52‰ for KI to +0.50‰ for K_2CO_3·1.5H_2O (Table 1, Fig. 2). It is important to note that $^{41}\Delta K_{min\text{-}aq}$

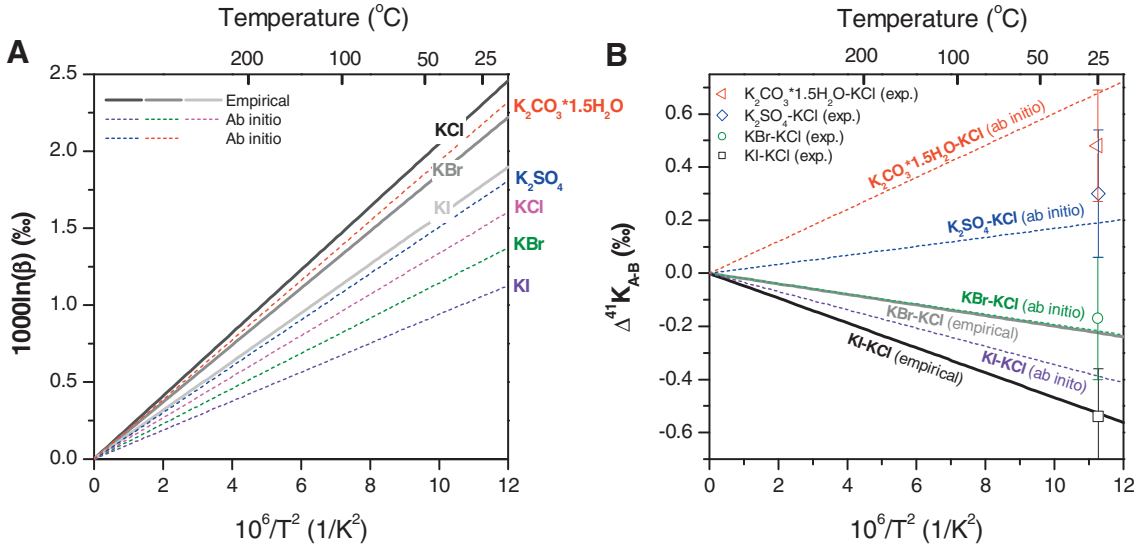

Fig. 3. Reduced partition function ratios (RPFRs or β factors) of K isotopes for K salts (A), and inter-mineral K isotope fractionation factors (B) as a function of temperature, based on empirical crystal chemistry models (solid lines) and *ab initio* calculations (dotted lines). For inter-mineral K isotope fractionation, solid or dashed lines in (B) denote fractionation factors derived from calculated β factors as in (A). The open symbols with error bars denote inter-mineral fractionation between pairs that are calculated based on $\Delta^{41}K_{min\text{-}aq}$ factors measured from recrystallization experiments, assuming saturated K solutions have the same β factor for K. Errors denote 2SD and are propagated from analytical uncertainties of individual minerals and aqueous solutions in Table 1. See discussion for details.

factors show strong correlations with the average distance between K atoms and the nearest atoms of negative charge such as halogen and oxygen (termed as *r* hereafter). For example, if the salts are divided into those with anion complexes with a −1 charge (halides and bicarbonate) and those with anion complexes with a −2 charge, there is a strong negative correlation between the fractionation factor and *r* for each group (Fig. 2). The first group has monovalent anions, including $KHCO_3$ and the three K halides that have relative long K-halogen distance up to 3.53 Å. The second group includes the other four K-salts with divalent anions, in these salts K atoms are surrounded by O atoms as polyhedrons, and the average *r* are shorter and all below 3 Å. The two groups define different trends in the $^{41}\Delta K_{min\text{-}aq}$-*r* plot (Fig. 2). Particularly, the slope for K-halide trend (−1.3‰/Å) is about one third of the slope for divalent anion salt trend (−4.3‰/Å). It should be noted that crystal structure of the K-halides is fundamentally different as compared to $KHCO_3$ as well as other salt with complex anions. The lattice three K-halides are all of the highly symmetrical face-centered cubic structure (space group Fm3m), and the bonds in these halides are ionic; in contrast, symmetry is of much lower order in the $KHCO_3$ lattice (monoclinic, $P2_1/a$), where hydrogen bond of HCO_3^- anion plays an important role in atomic arrangement and the CO_3^{2-} group is remarkably distorted due to the hydrogen bond (Nitta et al., 1952). Additionally, K-halides are different from other K-salts by the fact that the K atoms in the non-halide K-salts are located in polyhedrons of oxygen atoms (Fig. 1), which should result in a different relationship between *r* and bond strength than the K-halide. Therefore, although $KHCO_3$ plots along the trend with the halides, it is not included in the following discussion.

The general negative correlation between $^{41}\Delta K_{min\text{-}aq}$ fractionation and *r* is consistent with theories of equilibrium stable isotope fractionation that predict preferential partitioning of heavy isotopes into phases with shorter, stronger chemical bonds (Bigeleisen and Mayer, 1947; O'Neil, 1986; Chacko et al., 2001; Schauble, 2004). However, there are finer patterns of correlation between isotopic fractionation and *r* as revealed in this study (Fig. 2), which are discussed below. Specifically, the three K halides (KCl, KBr, and KI) are iso-structural in lattice configurations, thus these salts provide a rare opportunity to analyze the bond length effect on isotope fractionation without complexities from other variables. Inter-mineral K isotope fractionation between the halides are estimated using the experimentally determined fluid-mineral fractionation factors. For example, taking the difference between the $\Delta^{41}K_{KI\text{-}aq}$ and the $\Delta^{41}K_{KCl\text{-}aq}$, a $\Delta^{41}K_{KCl\text{-}KI}$ of 0.54‰ is derived. Similarly, a $\Delta^{41}K_{KCl\text{-}KBr}$ of 0.17‰ is calculated. It should be noted that such treatment (e.g., $\Delta^{41}K_{KI\text{-}KCl} = \Delta^{41}K_{KI\text{-}aq} - \Delta^{41}K_{KCl\text{-}aq}$) is based on an assumption that the saturated K halide solutions have the same β values. β value of an element in aqueous solution is dependent on hydration number of ions (Rustad et al., 2010) and speciation of ions (Schott et al., 2016). Ion pairs and ion clusters become the major species of K in highly concentrated K solutions (Chen and Pappu, 2007), however, a quantitative assessment of proportion of ion pair and ion clusters for K in different saturated K salt solutions as well as their isotopic effects is beyond the scope of this study. Nevertheless, by assuming identical β values for different saturated K solutions it is possible to directly compare the results of the experiments to the theoretically calculated fractionation factors.

Our ab initio calculations predict that under equilibrium condition at 25 °C, $\delta^{41}K$ of KI and KBr is 0.45‰ and 0.21‰ lower than that of KCl, respectively, whereas $\delta^{41}K$ of $K_2CO_3{\cdot}1.5H_2O$ and K_2SO_4 is 0.67‰ and 0.19‰ higher than that of KCl, respectively (Table 3, Fig. 3). For comparison, calculations based on empirical crystal chemistry models show that at 25 °C, $\delta^{41}K$ of KI and KBr is 0.52‰ and 0.22‰ lower than that of KCl, respectively (Table 3, Fig. 3). There is an excellent agreement in the calculated inter-halides K isotope fractionation factors between the two different methods, although there are systematic differences in calculated β values for the salts between the two methods (Fig. 3a). Moreover, these calculated inter-salt fractionation factors are also in agreement with the results from the salt recrystallization experiments within analytical uncertainties (Fig. 3b). The consistency between results of laboratory experiments and theoretical calculations can support the validity of assuming similar β values for saturated K halide solutions despite the complexities in K speciation and related isotopic effects. Further, the apparent success of the empirical calculation for isotope fractionation calculation that is based on the relatively simple crystal-chemistry models using Born-Mayer function and Madelung constant may reside in the fact that these salts are type examples of ionic bonds and the crystal lattice of these salts are similar and with high degrees of symmetry.

Compared to *ab initio* approaches that require significant computational resources, the crystal chemistry model provides a more intuitive way for understanding the controlling factors of isotope fractionation via formulations with key parameters (Young et al., 2015). Particularly, Eq. (7) indicates that inter-mineral isotope fractionation is proportional to differences in force constants, and Eq. (10) indicates that force constant is a function of charge of the anions and cations ($Z^+ \times Z^-$), and bond length ($1/r^3$), in addition to mineral-dependent constants of M and n. In the $^{41}\Delta K_{min\text{-}aq}$-r plot (Fig. 2), K-halides trend has a slope that is about 1/3 of the other K-salts. The valence of oxygen is twice of the valence of halogen, and there is an additional 50% difference in $1/r^3$ between the two groups of minerals ($1/2.9^3$ versus $1/3.3^3$, taking the medium *r* of the two groups for calculation). Therefore, the difference in slopes of the trends between K-halides and non-halide salts in Fig. 2 can be satisfactorily explained by a combination of charge (valence) and inter-atomic distance (*r*). Fundamentally, K isotope fractionations between salts are controlled by their crystal-chemistries.

4.3. Potential applications

As products of brine evaporation, evaporites are ubiquitous on Earth throughout geological history and evaporites are an important constituent in sedimentary sequences in enclosed basins. Precipitation of K-salts from brines always occurs at the late stages of evaporation, generally after precipitation of carbonate, gypsum, and halite (Bąbel and Schreiber, 2014). The assemblage of minerals precipitated in the final stages of brine evaporation is dependent on the initial solution chemistry (Eugster, 1980), and can be divided into the $MgSO_4$-poor potash evaporites group and the $MgSO_4$-rich potash evaporite group (Hardie, 1991). The abundance of $MgSO_4$-poor potash evaporite is much greater than that of $MgSO_4$-rich potash evaporite in sedimentary records (Bąbel and Schreiber, 2014), and occurrence of $MgSO_4$-rich potash evaporite is confined to the Permian the Tertiary whereas $MgSO_4$-poor potash evaporite deposits occurred throughout the Phanerozoic (Hardie, 1990).

Potassium salts in $MgSO_4$-poor potash evaporites include sylvite (KCl) and carnallite ($MgCl_2{\cdot}KCl{\cdot}6H_2O$) (Hardie, 1991). Ancient $MgSO_4$-poor potash evaporite sequences commonly started with sylvite and was followed by carnallite, which was experimentally confirmed for SO_4^{2-} depleted brines (Hadzeriga, 1967; Valyashko, 1972; Bąbel and Schreiber, 2014). Because sylvite is the first K phase to be crystallized from SO_4^{2-} depleted brines and based on the experiments presented here that show there is no measurable fractionation between K solutions and sylvite, it should be possible to use the K isotope composition of sylvite to infer aqueous K isotope compositions. Moreover, due to the negligible K isotope fractionation between KCl and saturated aqueous solution, fractional crystallization of sylvite will not change the K isotope composition of brine, thus K isotope compositions of primary syndepositional sylvite should be invariant. Therefore, homogeneous K isotope compositions of sylvite samples from the same $MgSO_4$-poor potash evaporite deposit could be a useful indicator for tracing K isotope compositions of brines in a sedimentary basin.

In $MgSO_4$-rich potash evaporites, the K-salts include kainite ($MgSO_4{\cdot}KCl{\cdot}11/4H_2O$) and polyhalite ($2CaSO_4{\cdot}MgSO_4{\cdot}K_2SO_4{\cdot}2H_2O$), in addition to sylvite and carnallite (Hardie, 1991). In the mineral precipitation sequence for $MgSO_4$-rich potash evaporites, polyhalite and kainite commonly occur as the first K-bearing minerals to be precipitated (McCaffrey et al., 1987; Warren, 2006), although sylvite could also be precipitated after polyhalite in the $MgSO_4$-rich potash evaporite sequence, given certain solution chemistry (Spencer and Hardie, 1990). Wang and Jacobsen (2016a) reported that $\delta^{41}K$ of late Permian sylvite from southern United States is similar to that of modern seawater, but $\delta^{41}K$ of late Permian sylvite from Germany is 0.13‰ higher than that of modern seawater. Because Permian evaporites belong to the $MgSO_4$-rich potash evaporite group, sylvite samples analyzed by Wang and Jacobsen (2016a) are unlikely to be the first K-bearing phase that was separated from brines in the precipitation sequence, therefore one cannot deduce the K isotope composition of initial seawater based on the currently available data. This is supported by the difference in K isotope data from the two salt samples, which could be caused by modification of K isotope composition of the brine by variable degree of polyhalite precipitation, or mixing with other solute sources in the two basins.

Based on the discussions above, we suggest that it is possible to track the K isotope composition of seawater or brine and to constrain the evaporation history of restricted basin through time by analysis of K isotope composition of K-bearing salts (e.g., sylvite) evaporite deposits. The full potential of K isotopes in evaporite research is yet to be

exploited by more systematic analysis of K isotope compositions of K-salts in evaporites, and determination of K isotope fractionation factors for relevant complex salts, such as kainite, polyhalite, and carnallite, as well as a better understanding of the effect of solution chemistry (cation and anion species and concentration) on K isotope partitioning in future studies.

5. CONCLUSIONS

Recrystallization experiments for eight K-salts were conducted to determine the equilibrium K isotope fractionation factor between the salt and the respective saturated aqueous solution at 25°C. The K isotope fractionation factors ($\delta^{41}K_{solid}$-$\delta^{41}K_{aquous}$) are 0.50‰ for $K_2CO_3 \cdot 1.5H_2O$, 0.32‰ for K_2SO_4, 0.23‰ for $KHCO_3$, 0.06‰ for $K_2C_2O_4 \cdot H_2O$, 0.02‰ for KCl, −0.03‰ for K_2CrO_4, −0.15‰ for KBr, and −0.52‰ for KI. On the other hand, *ab initio* calculations yielded inter-mineral K isotope fractionations of −0.22‰ for $\ln\alpha_{KBr\text{-}KCl}$, −0.45‰ for $\ln\alpha_{KI\text{-}KCl}$, 0.19‰ for $\ln\alpha_{K2SO4\text{-}KCl}$, and 0.51‰ for $\ln\alpha_{K2CO3\text{-}KI}$ at 25 °C. Using empirical crystal-chemistry models, we calculated inter-mineral K isotope fractionation factors between K-halides, which are −0.22‰ for $\ln\alpha_{KBr\text{-}KCl}$, and −0.52‰ for $\ln\alpha_{KI\text{-}KC}$ at 25 °C. The calculated inter-mineral K isotope fractionation factors are in good agreement with offsets between measured mineral-solution fractionation factors for the halides, although we note that experimentally derived inter-mineral K isotope fractionation factors are calculated based on an assumption of consistent β factors for different saturated K solutions, which has not been proven yet.

Experimental data show that $\Delta^{41}K_{min\text{-}sol}$ decreases with increasing *r* for K in crystals, where *r* is the average distance between K atom and the neighboring atoms of negative charge. Furthermore, K isotope fractionation for halides is three times less sensitive to change in *r* than the non-halide salts of divalent anions. This is satisfactorily explained by charge difference in anions and the difference in *r*, the later correlate with fractionation factor following a rule of $1/r^3$.

Sylvite is an important constituent in evaporites, and is commonly the first K-bearing phases to be crystallized from the brine during evaporation in the $MgSO_4$-poor potash evaporites. Therefore it is possible to track K isotope composition of ancient brines using K isotopes in sylvite based on the experimentally determined K isotope fractionation factors for KCl in this study. More experimental calibrations of K isotope fractionation factors during precipitation of kainite, polyhalite, and carnallite are needed for better understanding of K isotopes in evaporites in future studies.

ACKNOWLEDGEMENTS

This manuscript benefits from constructive reviews from three anonymous reviewers. We also thank Dr. Fangzhen Teng for his editorial handling and constructive comments. Yongjiang Xu assisted in taking photos for the crystals, Yang Zhang assisted in XRD analysis. The numerical calculations in this paper have been done on the computing facilities in the High Performance Computing Center of Nanjing University. This study was supported by the DREAM project of Ministry of Science and Technology of China (Project No. 2017YFC0602801) and National Science Foundation of China (Grant No. 41622301) to WL. KDK acknowledges the support from the National Research Foundation of Korea (NRF-2016R1D1A1B03931919). This study was also supported by the NASA Astrobiology Institute (grant NNA13AA94A to BLB.).

APPENDIX A. SUPPLEMENTARY MATERIAL

Supplementary data associated with this article can be found, in the online version, at http://dx.doi.org/10.1016/j.gca.2017.07.037.

REFERENCES

Ackland G. J., Warren M. C. and Clark S. J. (1997) Practical methods in ab initio lattice dynamics. *J. Phys.: Condens. Matter* **9**, 7861.

Ahtee M. (1969) Lattice constants of some binary alkali halide solid solutions. *Annales Academiae Scientiarum Fennicae Series A6: Physica* **313**, 1–11.

Bąbel M. and Schreiber B. C. (2014) 9.17 - geochemistry of evaporites and evolution of seawater A2 - Holland, Heinrich D. In *Treatise on Geochemistry* (ed. K. K. Turekian), second ed. Elsevier, Oxford, pp. 483–560.

Barnes I. L., Garner E. L., Gramlich J. W., Machlan L. A., Moody J. R., Moore L. J., Murphy T. J. and Shields W. R. (1973) Isotopic abundance ratios and concentrations of selected elements in some Apollo 15 and Apollo 16 samples. *Lunar Planet. Sci. Conf. Proc.* **2**, 1197–1207.

Baroni S., de Gironcoli S., Dal Corso A. and Giannozzi P. (2001) Phonons and related crystal properties from density-functional perturbation theory. *Rev. Mod. Phys.* **73**, 515–562.

Berner R. A. (1978) Rate control of mineral dissolution under Earth surface conditions. *Am. J. Sci.* **278**, 1235–1252.

Bigeleisen J. and Mayer M. G. (1947) Calculation of equilibrium constants for isotopic exchange reactions. *J. Chem. Phys.* **15**, 261–267.

Blanchard M., Poitrasson F., M閔eut M., Lazzeri M., Mauri F. and Balan E. (2009) Iron isotope fractionation between pyrite (FeS_2), hematite (Fe_2O_3) and siderite ($FeCO_3$): a first-principles density functional theory study. *Geochim. Cosmochim. Acta* **73**, 6565–6578.

Born M. and Mayer J. E. (1932) Zur Gittertheorie der Ionenkristalle. *Zeitschrift für Physik* **75**, 1–18.

Broecker W. S. and Peng T. H. (1982) *Tracers in the Sea*. Lamont-Doherty Earth Obs, Palisades, N.Y..

Chacko T., Cole D. R. and Horita J. (2001) Equilibrium oxygen, hydrogen and carbon isotope fractionation factors applicable to geologic systems. In *Stable Isotope Geochemistry* (eds. J. W. Valley and D. R. Cole). The Mineralogical Society of America, Washington DC, pp. 1–82.

Chen A. A. and Pappu R. V. (2007) Quantitative characterization of ion pairing and cluster formation in strong 1:1 electrolytes. *J. Phys. Chem. B* **111**, 6469–6478.

Clark S. J., Segall M. D., Pickard C. J., Hasnip P. J., Probert M. I. J., Refson K. and Payne M. C. (2005) First principles methods using CASTEP. *Zeitschrift Fur Kristallographie* **220**, 567–570.

DePaolo D. J. (2011) Surface kinetic model for isotopic and trace element fractionation during precipitation of calcite from aqueous solutions. *Geochim. Cosmochim. Acta* **75**, 1039–1056.

Dove M. T. (1993) *Introduction to Lattice Dynamics*. Cambridge University Press, Cambridge.

Eugster H. P. (1980) Geochemistry of evaporitic lacustrine deposits. *Annu. Rev. Earth Planet. Sci.* **8**, 35–63.

Francis G. P. and Payne M. C. (1990) Finite basis set corrections to total energy pseudopotential calculations. *J. Phys.: Condens. Matter* **2**, 4395.

Garner E. L., Machalan L. A. and Barnes I. L. (1975) The isotopic composition of lithium, potassium, and rubidium in some Apollo 11, 12, 14, 15, and 16 samples. *Lunar Planet. Sci. Conf. Proc.* **6**, 1845–1855.

Hadzeriga P. (1967) Dynamic equilibria in the solar evaporation of the Great Salt Lake brine. *Trans. Soc. Min. Eng. AIME* **238**, 413–419.

Hardie L. A. (1990) The roles of rifting and hydrothermal $CaCl_2$ brines in the origin of potash evaporites: an hypothesis. *Am. J. Sci.* **290**, 43–106.

Hardie L. A. (1991) On the significance of evaporites. *Annu. Rev. Earth Planet. Sci.* **19**, 131–168.

Humayun M. and Clayton R. N. (1995a) Potassium isotope cosmochemistry: Genetic implications of volatile element depletion. *Geochim. Cosmochim. Acta* **59**, 2131–2148.

Humayun M. and Clayton R. N. (1995b) Precise determination of the isotopic composition of potassium: Application to terrestrial rocks and lunar soils. *Geochim. Cosmochim. Acta* **59**, 2115–2130.

Humayun M. and Koeberl C. (2004) Potassium isotopic composition of Australasian tektites. *Meteorit. Planet. Sci.* **39**, 1509–1516.

Kieffer and Werner S. (1982) Thermodynamics and lattice vibrations of minerals: 5. Applications to phase equilibria, isotopic fractionation, and high-pressure thermodynamic properties. *Rev. Geophys.* **20**, 827–849.

Kleinman L. and Bylander D. M. (1982) Efficacious form for model pseudopotentials. *Phys. Rev. Lett.* **48**, 1425–1428.

Lasaga, A.C., 1981. Rate laws of chemical reactions. In: Lasaga, A. C., Kirkpatrick, R.J. (Eds.), Reviews in Mineralogy, pp. 1–68.

Lasaga, A.C., 1990. Atomic treatment of mineral-water surface reactions. Reviews in Mineralogy and Geochemistry V23: Mineral-water interface geochemistry, 17–86.

Lemarchand D., Wasserburg G. J. and Papanastassiou D. A. (2004) Rate-controlled calcium isotope fractionation in synthetic calcite. *Geochim. Cosmochim. Acta* **68**, 4665–4678.

Li W. (2017) Vital effects of K isotope fractionation in organisms: observations and a hypothesis. *Acta Geochim.*. http://dx.doi.org/10.1007/s11631-11017-10167-11631.

Li W., Beard B. L. and Johnson C. M. (2011) Exchange and fractionation of Mg isotopes between epsomite and saturated $MgSO_4$ solution. *Geochim. Cosmochim. Acta* **75**, 1814–1828.

Li W., Beard B. L. and Li S. (2016) Precise measurement of stable potassium isotope ratios using a single focusing collision cell multi-collector ICP-MS. *J. Anal. At. Spectrom.* **31**, 1023–1029.

Lyubetskaya T. and Korenaga J. C. B. (2007) Chemical composition of Earth's primitive mantle and its variance: 1. Method and results. *J. Geophys. Res.: Solid Earth* **112**. http://dx.doi.org/10.1029/2005JB004223.

McCaffrey M. A., Lazar B. and Holland H. D. (1987) The evaporation path of seawater and the coprecipitation of Br - and K + with halite. *J. Sediment. Petrol.* **57**, 928–937.

McGinnety J. A. (1972) Redetermination of the structures of potassium sulphate and potassium chromate: the effect of electrostatic crystal forces upon observed bond lengths. *Acta Crystallogr. Sect. B* **28**, 2845–2852.

Mei W. N., Boyer L. L., Mehl M. J., Ossowski M. M. and Stokes H. T. (2000) Calculation of electronic, structural, and vibrational properties in alkali halides using a density-functional method with localized densities. *Phys. Rev. B* **61**, 11425–11431.

Meybeck M. (2003) Global occurrence of major elements in rivers. *Treatise on geochemistry. Elsevier*, 207–223.

Michalopoulos P. and Aller R. C. (1995) Rapid clay mineral formation in amazon delta sediments: reverse weathering and oceanic elemental cycles. *Science* **270**, 614–617.

Monkhorst H. J. and Pack J. D. (1976) Special points for Brillouin-zone integrations. *Phys. Rev. B* **13**, 5188–5192.

Nitta I., Tomiie Y. and Koo C. H. (1952) The crystal structure of potassium bicarbonate, $KHCO_3$. *Acta Crystallogr. A* **5**, 292-292.

O'Neil J. R. (1986) Theoretical and experimental aspects of isotopic fractionation. *Rev. Mineral.* **16**, 1–40.

Palme H. and O'Neill H. S. C. (2014) *Cosmochemical Estimates of Mantle Composition, Treatise on Geochemistry*, second ed. Elsevier, Oxford, pp. 1–39.

Parendo C. A., Jacobsen S. B. and Wang K. (2017) K isotopes as a tracer of seafloor hydrothermal alteration. *Proc. Natl. Acad. Sci.* **114**, 1827–1831.

Perdew J. P., Burke K. and Ernzerhof M. (1997) Generalized gradient approximation made simple. *Phys. Rev. Lett.* **77**, 3865–3868.

Pfrommer B. G., Côté M., Louie S. G. and Cohen M. L. (1997) Relaxation of crystals with the Quasi-Newton method. *J. Comput. Phys.* **131**, 233–240.

Refson K., Tulip P. R. and Clark S. J. (2006) Variational density-functional perturbation theory for dielectrics and lattice dynamics. *Phys. Rev. B* **73**, 155114.

Richter F. M., Mendybaev R. A., Christensen J. N., Ebel D. and Gaffney A. (2011) Laboratory experiments bearing on the origin and evolution of olivine-rich chondrules. *Meteorit. Planet. Sci.* **46**, 1152.

Rudnick R. L. and Gao S. (2003) Composition of the continental crust. In *Treatise on Geochemistry* (eds. H. D. Holland and K. K. Turekian). Elsevier, pp. 1–64.

Ruffa A. R. (1980) Empirical determination of thermal expansion in insulators with no experimental input. *J. Mater. Sci.* **15**, 2268–2274.

Rustad J. R., Casey W. H., Yin Q.-Z., Bylaska E. J., Felmy A. R., Bogatko S. A., Jackson V. E. and Dixon D. A. (2010) Isotopic fractionation of Mg^{2+}(aq), Ca^{2+}(aq), and Fe^{2+}(aq) with carbonate minerals. *Geochim. Cosmochim. Acta* **74**, 6301–6323.

Sakamoto Y. (1958) Madelung constants of simple crystals expressed in terms of Born's basic potentials of 15 figures. *J. Chem. Phys.* **28**, 164–165.

Schauble E. A. (2004) *Applying stable isotope fractionation theory to new systems, Geochemistry of Non-Traditional Stable Isotopes*. Mineralogical Soc America, Washington, pp. 65–111.

Schauble E. A., Ghosh P. and Eiler J. M. (2006) Preferential formation of 13 C–18O bonds in carbonate minerals, estimated using first-principles lattice dynamics. *Geochim. Cosmochim. Acta* **70**, 2510–2529.

Schott J., Mavromatis V., Fujii T., Pearce C. R. and Oelkers E. H. (2016) The control of carbonate mineral Mg isotope composition by aqueous speciation: theoretical and experimental modeling. *Chem. Geol.* **445**, 120–134.

Skakle J. M. S., Wilson M. and Feldmann J. (2001) Dipotassium carbonate sesquihydrate: rerefinement against new intensity data. *Acta Crystallogr. Sect. E* **57**, i94–i97.

Spencer R. J. and Hardie L. A. (1990) Control of seawater composition by mixing of river waters and mid-ocean ridge hydrothermal brines. *Spec. Publ. - Geochem. Soc.* **19**, 409–419.

Spivack A. J. and Staudigel H. (1994) Low-temperature alteration of the upper oceanic crust and the alkalinity budget of seawater. *Chem. Geol.* **115**, 239–247.

Stoffregen R. E., Rye R. O. and Wasserman M. D. (1994) Experimental studies of alunite: II. Rates of alunite-water alkali and isotope exchange. *Geochim. Cosmochim. Acta* **58**, 917–929.

Teng F.-Z., Dauphas N. and Watkins J. M. (2017) Non-traditional stable isotopes: retrospective and prospective. *Rev. Mineral. Geochem.* **82**, 1–26.

Urey H. C. (1947) The thermodynamic properties of isotopic substances. *J. Chem. Soc.*, 562–581.

Valyashko, M.G., 1972. Scienfitic works in the field of geochemistry and the genesis of salt deposits in the U.S.S.R. In: Richter-Bernburg, G. (Ed.), Geology of Saline Deposits. Proceedings of the Hanover Symposium 15–21 May 1968. United Nations Educational, Scientific and Cultural Organization, Paris, pp. 289–311.

Walker D., Verma P. K., Cranswick L. M. D., Jones R. L., Clark S. M. and Buhre S. (2004) Halite-sylvite thermoelasticity. *Am. Miner.* **89**, 204.

Wang K. and Jacobsen S. B. (2016a) An estimate of the Bulk Silicate Earth potassium isotopic composition based on MC-ICPMS measurements of basalts. *Geochim. Cosmochim. Acta* **178**, 223–232.

Wang K. and Jacobsen S. B. (2016b) Potassium isotopic evidence for a high-energy giant impact origin of the Moon. *Nature* **538**, 487–490.

Warren, J.K., 2006. Evaporites: Sediments, resources and hydrocarbons.

Young E. D., Galy A. and Nagahara H. (2002) Kinetic and equilibrium mass-dependent isotope fractionation laws in nature and their geochemical and cosmochemical significance. *Geochim. Cosmochim. Acta* **66**, 1095–1104.

Young E. D., Manning C. E., Schauble E. A., Shahar A., Macris C. A., Lazar C. and Jordan M. (2015) High-temperature equilibrium isotope fractionation of non-traditional stable isotopes: experiments, theory, and applications. *Chem. Geol.* **395**, 176–195.

Young E. D., Tonui E., Manning C. E., Schauble E. and Macris C. A. (2009) Spinel-olivine magnesium isotope thermometry in the mantle and implications for the Mg isotopic composition of Earth. *Earth Planet. Sci. Lett.* **288**, 524–533.

Associate editor: Fang-Zhen Teng